

# RELATING OCEAN SURFACE WIND AND RAIN

191

Wenqing Tang\* and W. Timothy Liu  
Jet Propulsion Laboratory, California Institute of Technology

## 1. INTRODUCTION

The decade long data from the Tropical Rain Measuring Mission (TRMM) and SeaWinds on QuikSCAT provide new perspectives to the interaction between wind and rain in the diurnal cycle and tropical cyclone. The low inclination orbit and frequent sampling of TRMM have provided us with reliable observation on rain diurnal cycle (Imaoka and Spencer, 2000; Lau et al, 2007). Frequent sampling of ocean surface wind vector was provided by a six-month (from April 10 to October 24, 2003) tandem mission when two identical scatterometers SeaWinds were flown on NASA QuikSCAT (QS) and Japanese Midori-2 (SW) satellites, with different local crossing times of 5:54am and 10:30pm respectively for the ascending nodes. These two data sets allow us to compare and relate the diurnal cycles of wind and rain. The wide-swath sensors, like the scatterometer and microwave radiometer also provide the opportunity to observe the surface structure and asymmetry of tropical cyclones. The decade-long observations provide statistical significant ensemble of tropical cycles to examine how the translation speed induced asymmetry affects the intensification of the storm under different environmental conditions.

## 2. DIURNAL CYCLE OF RAIN AND WIND OVER OCEANS

Observing the large-scale diurnal variability in ocean surface rain and wind is crucial to understanding the fundamental mechanisms controlling the day-night changes of a variety of elements, for example, cloudiness and air-sea fluxes exchanges. Rain data used in this study is extracted from the version-4 TRMM/TMI ocean products from the Remote Sensing System (<http://ssmi.com>). Daily surface rain rate was binned into 24-hour local time bins over global oceans on  $0.5^\circ \times 0.5^\circ$  grid, and averaged over one year period. The amplitude (A1) and phase (P1) of the rain diurnal cycle were derived over each grid point from the binned data for each year from 2000 to 2010. The ensemble of eleven maps of A1 and P1 will be used

\*Corresponding author address: Wenqing Tang, 4800 Oak Grove Drive, Jet Propulsion Laboratory, MS 300-323, Pasadena, CA 91109; e-mail: Wenqing.tang@jpl.nasa.gov

to estimate the uncertainties. Figure 1a shows the ensemble average of A1. Strong diurnal cycle in rain was observed in the coastal area in south east Asia, in the Intertropical Convergence Zones (ITCZ), and in regions known largely effected by topography. Uncertainties of A1 are presented as the standard deviation of the ensemble (Fig.1b). It is noticed that the uncertainty level in regions where strong A1 observed as mentioned above is comparable with vicinity, indicating the persistence and reliability of observed feature. Maps of P1, the local peak time of the diurnal cycle (Fig. 1c), and the ensemble spread of P1, defined as the difference between the maximum and minimum values of P1 (Fig. 1d), reveal that ocean surface is dominated by morning rain, with uncertainty around 3 hours.

Rain should be closely related to surface wind convergence at short time scales through convection over tropical oceans. Current knowledge on the wind diurnal cycle is mainly based on in situ measurements (e.g. Deser and Smith, 1998; Dai and Deser, 1999), which usually have temporal sampling frequency up to hourly but sparse in spatial distribution. Assessments on the large-scale spatial pattern should greatly benefit from satellite remote sensing. Using ocean vector wind data from the scatterometer, Gille et al (2003, 2005) analyzed the differences between morning and evening measurements and identified a significant signal associated with sea breeze along the world coastlines. We constructed ocean surface wind diurnal cycle combining six-month data from QS and SW. Wind convergence was calculated from zonal and meridional wind components provided in the level 2 products (accessible from <http://podaac.jpl.nasa.gov>), and binned to  $0.5^\circ \times 0.5^\circ$  grid over global ocean for ascending and descending passes respectively. Averaged over the tandem mission period, we obtained four global maps at local satellite passing times. The amplitude (A1) and phase (P1) of diurnal cycle at each grid point was extracted through a simple first order harmonic fitting. From the A1 map (not shown), clear patterns of strong wind convergence can be found in the equatorial region and along coastlines which is known associated with sea breeze. It is noticed that strong diurnal amplitude in wind convergence is not necessarily matching with pattern of large rain diurnal variability, for example, along north- and south-west Australia, and along the west coast of Arabian Sea. This is likely associated with the fact that adjacent land is rather dry, but need

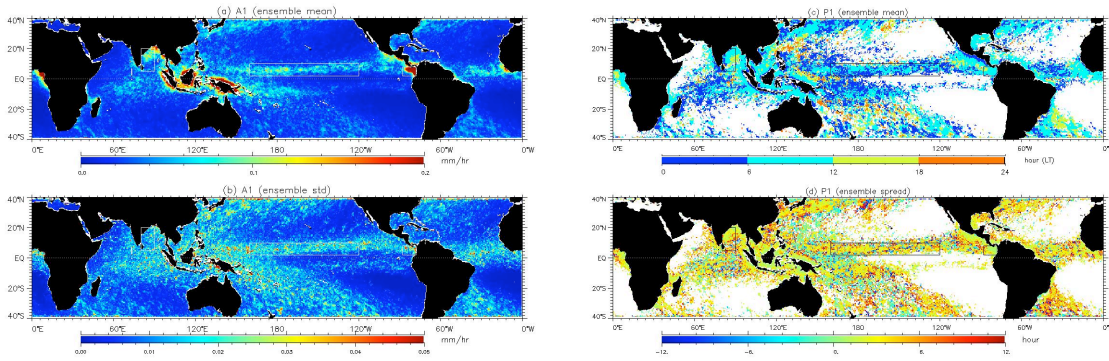


Figure 1. The ensemble mean of the rain diurnal cycle amplitude  $A1$  (a) and phase  $P1$  (c) derived from TRMM/TMI surface rainfall from 2000 to 2010.  $P1$  is shown as the local peak time (hour), with white indicates area where  $A1$  is less than 0.02 mm/hr. The uncertainty for  $A1$  (b) is the standard deviation of the ensemble, and the uncertainty for  $P1$  (d) is the ensemble spread (the difference between maximum and minimum peak time).

further investigation. What we are interested in this study is the linkage between rain and wind on the diurnal scale. To eliminate any potential seasonal effect, we recreated the rain diurnal cycle only using the TRMM/TMI data in the scatterometer tandem mission period. Figure 2 shows the local peak time for wind convergence and rain, in the area where rain diurnal variation exceeds 0.02 mm/hr. Figure 3 plots cycles of wind convergence and rain in a few regions. In the Bay of Bengal, the cycles of rain and wind convergence were found to be in phase. In the Pacific ITCZ, wind convergence peaks about 3 to 4 hours ahead of rain, while it is a few hours behind the rain offshore near Columbia. The underlying mechanism of these phase lags are being investigated.

### 3. THE WIND AND RAIN ASYMMETRY UNDER TROPICAL CYCLONES

The intensity change of tropical cyclone results from its interaction with the underneath ocean and atmospheric environment through momentum and energy exchanges. The convective cells organized at lower level uplift moisture, which return as precipitation and fuel energy back to the system as latent heat (Emanuel, 1986a, 1986b). The lack of understanding of the controlling mechanism is hindering hurricane intensity forecast; even though great improvement has been made on hurricane tracks over past several decades. Traditional hurricane observations were carried operationally by aircraft flying through cyclones or obtained from field

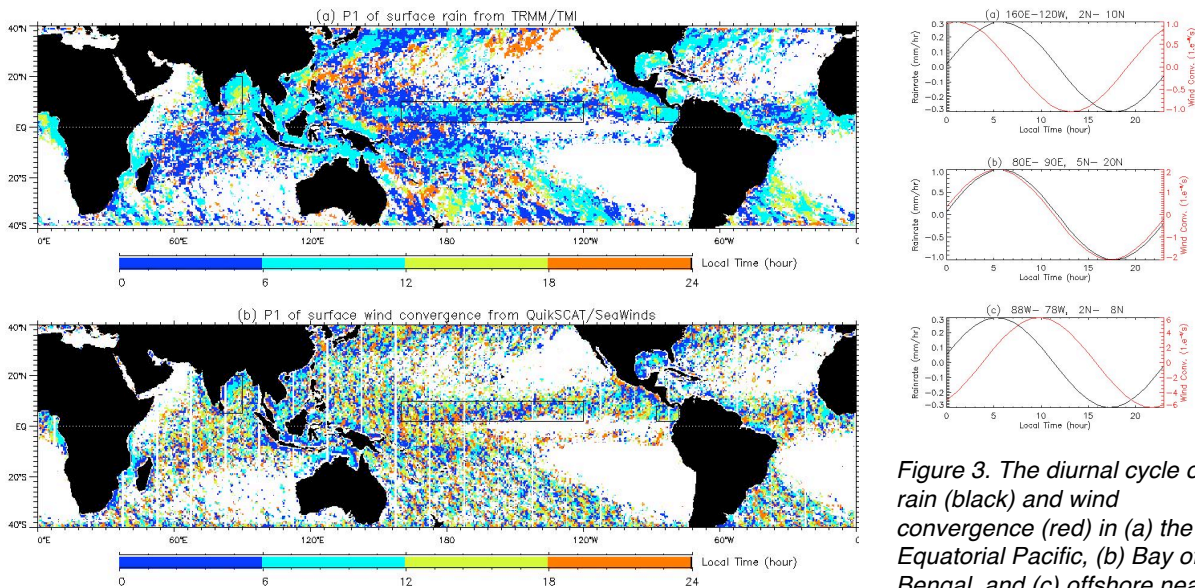


Figure 2. Local peak time of rain (a) and wind convergence (b) of the diurnal cycle, both derived using 6 months data from the scatterometer tandem mission period.

Figure 3. The diurnal cycle of rain (black) and wind convergence (red) in (a) the Equatorial Pacific, (b) Bay of Bengal, and (c) offshore near Columbia.

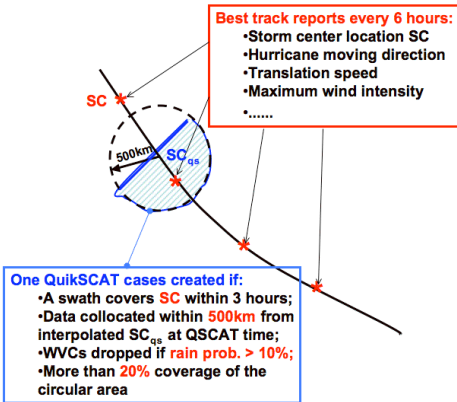


Figure 4. Schematic diagram for retrieving satellite data associated with tropical storms.

experiments. Those measurements are often intense along the flying path while unable to depict synoptic spatial variance. Spacebased instruments, from its vantage point of view, have the ability of taking the “snapshot” of the storm. Previous studies have used TRMM data and composite methodology to study the precipitation relative to storm motion (Lonfat et al, 2004) and vertical wind shear (Chen et al, 2006). We attempt to relate rain and wind under tropical cyclones and explore their impact on storm intensification through composite of synoptic maps stratified into different groups. Using over ten thousands scans of scatterometer measurements of tropical cyclones in eleven years over global oceans, we revealed the azimuthal asymmetry in radial velocity, tangential velocity, relative angular momentum input, and frictional drag. Wind asymmetry affects wind convergence asymmetry. Convergence causes the uplifting and rain. We are examining the relation between wind convergence and rain asymmetry with respect to hurricane intensification.

Database of tropical storms wind and rain was established by extracting data along the tracks of tropical storms from by QuikSCAT and TRMM/TMI for the period from July 1999 to November 2009. The best track analysis from the National Hurricane Center and the Joint Typhoon Warning Center for various ocean basins were used to extract satellite observation on tropical storms. As shown in Figure 4, for each of 6-hourly report along the best track, our search routine first identifies any QS orbits, which might contain data near storm center. Then the location of storm center (SC) corresponding to the measuring time of the selected QS orbit ( $X_{sc}$ ,  $Y_{sc}$ )<sub>QS-time</sub> in the storm region was interpolated from the two nearest points on the best track, along with ancillary information such as the maximum wind speed, storm moving direction, and translation speed. Figure 5 shows an example of the vector wind extracted from QS data, within 1000km from ( $X_{sc}$ ,  $Y_{sc}$ )<sub>QS-time</sub>. Wind

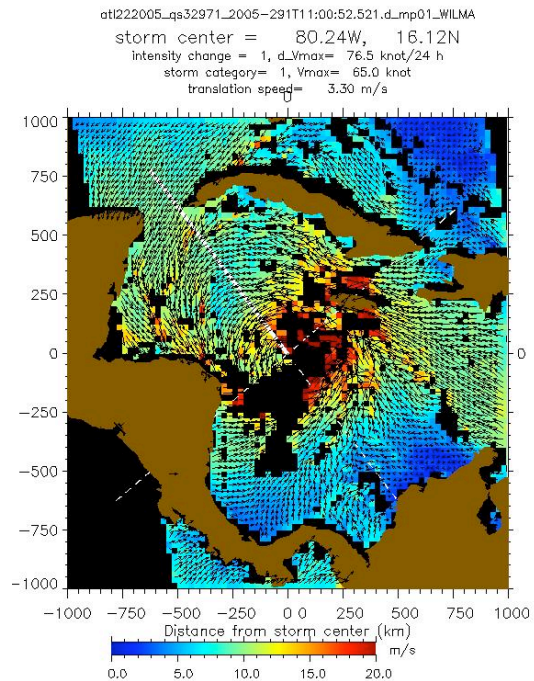


Figure 5. Example of wind extracted from QuikSCAT data. Inserted white lines divide 1000kmx1000km area around storm center into four quadrants, with the solid white line indicating the storm moving direction.

vector cells (WVCs) contaminated by rain were filtered out by eliminating records with more than 10% probability of detecting rain. A similar procedure was applied to extract TRMM/TMI rainfall under tropical storms. Table 1 lists the number of storm cases captured by QS and TRMM respectively for each year.

The hurricane wind/rain structure can be depicted from the composite of the QS- and TRMM-hurricane databases, obtained by averaging over all individual cases in the selected groups according specified selecting criteria. Composite is basically average of all cases within a group satisfying a set of pre-defined criteria, after each case in the group is rotated respectively so that the storm’s moving direction aligned with the positive y-axis. Note that for parameter to be composed that way it must be mathematically characterized as rotational invariant, which is satisfied by scalar variables such as rain rate, cloud, vapor, wind speed, but wind vector must be projected to cylindrical coordinates, i.e., in radial and tangential components. Composition can be performed in different stratified groups according to a set of specified criteria as long as the group contains enough ensembles to draw significant statistics. Figure 6 shows the composite of radial and tangential

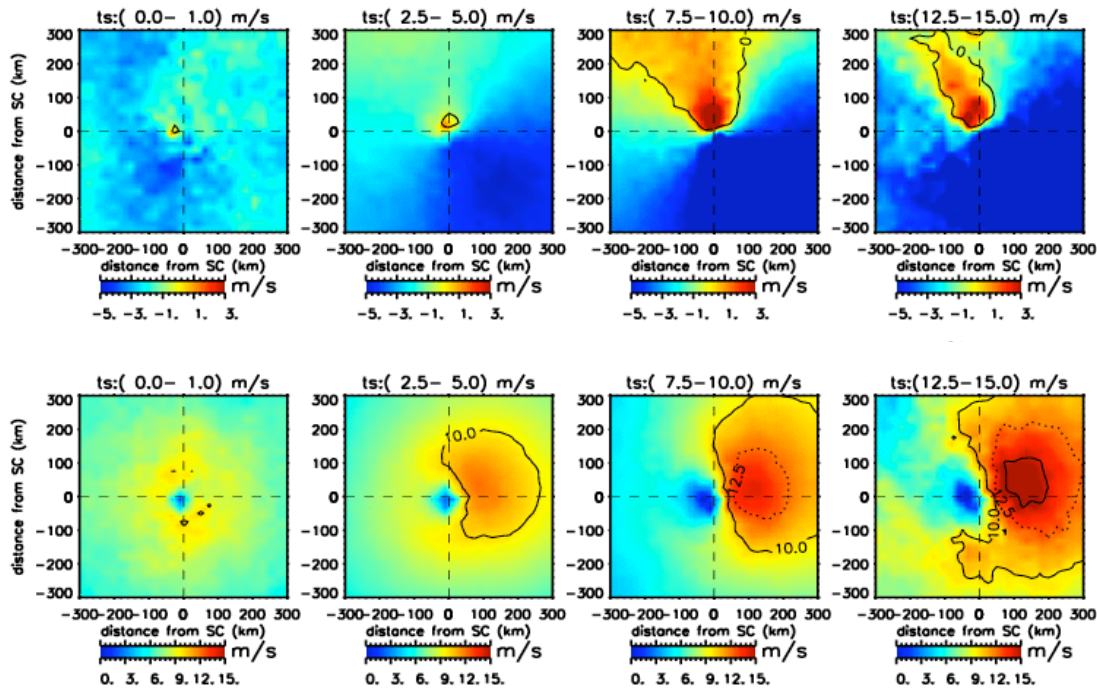


Figure 6. Composite of radial (top panel) and tangential (bottom panel) wind components in northern hemisphere from 2000 to 2007 measured by QuikSCAT, with various storm translation speeds (from left to right): 0-1, 2.5-5, 7.5-10, 12.5-15 m/s, where positive y-axis (up) aligned with storm moving direction and origin at the storm center. Contours in the plots indicate the zero value for the radial components and 10 m/s for tangential components.

wind components according to the storm translation speed. It reveals that radial wind component broadly inflows towards storm center with maximum from right-rear; and a narrow outflow in front to the left. Tangential wind component (and wind speed) is stronger on the right of storm track in Northern Hemisphere.

To explore the interaction between wind and rain, and their effect on storm intensification, we divided the database into groups according the tendency of storm

intensity change at the moment of satellite passes. If in the 24 hours period around satellite measurement, the maximum sustained wind increases more than 20 knots, we classify the case as “intensifying”; if it decreases more than 20 knots, we call the case “weakening”. Wavenumber-1 asymmetry maps were composed for intensifying and weakening respectively for wind convergence and rain. In northern hemisphere, as shown in Figure 7, the wind convergence is mostly largest ahead of storm motion for both intensifying and weakening groups, while rain

Table 1. Number of storm cases extracted from QuikSCAT and TRMM from 1999 to 2009.

QuikSCAT	1999	2000	2001	2002	2003	2004	2005	2006	2007	2008	2009	TOTAL
Atlantic	238	336	372	258	427	426	650	307	264	283	130	3691
E. Pacific	71	265	234	291	272	243	298	392	223	188	217	2694
N.W. Pacific	364	648	656	649	650	812	575	583	492	437	436	6302
N. Indian O.	10	52	61	49	63	99	86	59	69	20	6	574
S. Ocean	0	590	372	405	634	531	483	434	498	358	300	4605
<b>TOTAL</b>	<b>683</b>	<b>1891</b>	<b>1695</b>	<b>1652</b>	<b>2046</b>	<b>2111</b>	<b>2092</b>	<b>1775</b>	<b>1546</b>	<b>1286</b>	<b>1089</b>	<b>17866</b>
TRMM/TMI	1999	2000	2001	2002	2003	2004	2005	2006	2007	2008	2009	TOTAL
Atlantic	182	154	178	154	240	246	318	120	153	210	103	2058
E. Pacific	117	189	159	196	200	157	199	278	155	236	229	2115
N.W. Pacific	318	374	397	419	422	492	336	358	301	304	369	4090
N. Indian O.	55	40	39	33	45	70	79	57	54	67	33	572
S. Ocean	423	389	253	279	434	361	325	297	333	427	333	3854
<b>TOTAL</b>	<b>1095</b>	<b>1146</b>	<b>1026</b>	<b>1081</b>	<b>1341</b>	<b>1326</b>	<b>1257</b>	<b>1110</b>	<b>996</b>	<b>1244</b>	<b>1067</b>	<b>12689</b>

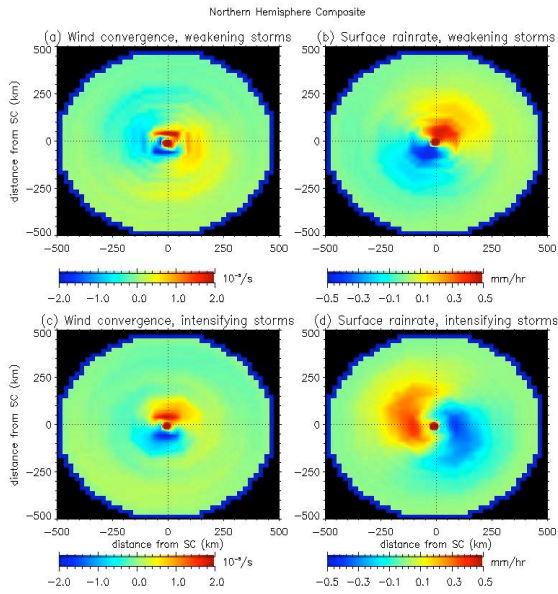


Figure 7. Northern hemisphere the wavenumber-1 asymmetry for weakening (top) and intensifying (bottom) storms for (a, c) wind-convergence and (b, d) surface rainrate, composed relative to the storm moving direction (positive y-axis).

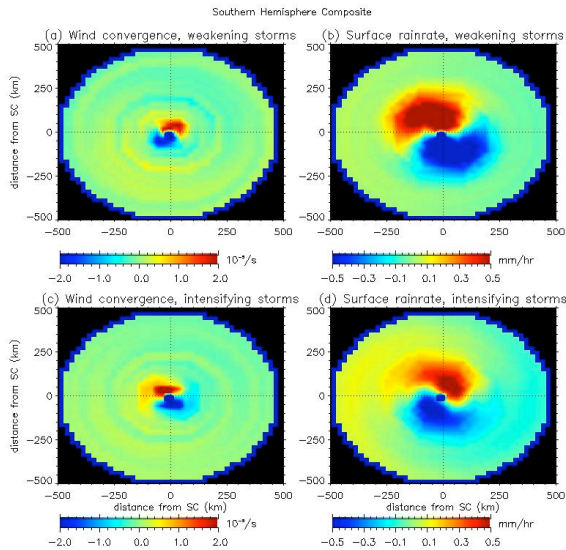


Figure 8. Similar as Fig. 7, composed for storms in the Southern Hemisphere.

is asymmetric relative to storm motion: most abnormal heavy rainfall happen in the left front quadrant for intensifying case, in right front quadrant for weakening case. Storms in southern hemisphere behave consistently as shown in Figure 8.

We propose the hypothesis that the relative positions of wind convergence behind of rain counter-clockwise (clockwise) in northern (southern) hemisphere, is in favor of storm intensifying (lower panels). When this relative position reversed, it favors storm weakening (upper panels). This will be further examined in conjunction with data from hurricane field campaign experiments to link the lower level wind convergence with upper atmospheric circulation, to better understand the dynamical processes controlling the intensity changes of tropical storms.

#### 4. REFERENCES

- Chen, S. S., J.A. Knaff, F. D. Marks, 2006: Effects of Vertical Wind Shear and Storm Motion on Tropical Cyclone Rainfall Asymmetries Deduced from TRMM, *Mon. Wea. Rev.*, 134, 3190-3208.
- Dai, A. and C. Deser, 1999: Diurnal and semidiurnal variation in global surface wind and divergence fields, *J. Geo. Res.*, 104, D24, 31109-31125.
- Deser, C. and C. A. Smith, 1998: Diurnal and semidiurnal variations of the surface wind field over the tropical Pacific Ocean, *J. of Clim.*, 11, 1730-1748.
- Emanuel, K. A., 1986a: An air-sea interaction theory for tropical cyclones. Part I: Steady-State Maintenance. *J. Atmos. Sci.*, 43, 585-604.
- Emanuel, K. A., 1986b: Some dynamical aspects of precipitating convection. *J. Atmos. Sci.*, 43, 2183-2198.
- Gille, S. T., S. G. L. Smith, and S. M. Lee, 2003: Measuring the sea breeze from QuikSCAT Scatterometry. *Geo. Res. Lett.*, 30(3), 1114, doi:10.1029/2002GL016230.
- Gille, S. T., S. G. Llewellyn Smith, and N. M. Statom, 2005: Global observations of the land breeze, *Geophys. Res. Lett.*, 32, L05605, doi:10.1029/2004GL022139.
- Imaoka, K., and R. W. Spencer, 2000: Diurnal variation of precipitation over the tropical oceans observed by TRMM/TMI combined with SSM/I. *J. of Clim.*, 13, 4149-4158.
- Lau, W. K. M, K. M. Kim, and M. I. Lee, 2007: Characteristics of diurnal and seasonal cycles in global monsoon systems. *J. of Meteor. Soc. of Japan*, 85A, 400-416.
- Lonfat, M., F. D. Marks, S. S. Chen, 2004: Precipitation Distribution in Tropical Cyclones Using the Tropical Rainfall Measuring Mission (TRMM) Microwave Imager: A Global Perspective, *Mon. Wea. Rev.*, 132, 1645-1660.